An experimental and computational study on soot formation in a coflow jet flame under microgravity and normal gravity

Bin Ma[1] Su Cao[1] Davide Giassi[1] Dennis P. Stocker[2] Fumiaki Takahashi[3]
Beth Anne V. Bennett[1] Mitchell D. Smooke[1] Marshall B. Long[1]

[1]Department of Mechanical Engineering & Materials Science, Yale University
New Haven, Connecticut 06511 USA
[2]NASA Glenn Research Center, Cleveland, Ohio 44135 USA
[3]National Center for Space Exploration Research, NASA Glenn Research Center
Cleveland, Ohio 44135 USA

Corresponding Author:

Bin Ma
Department of Mechanical Engineering and Materials Science
Yale University
New Haven, CT 06511
(203) 432-4229 (W)
(203) 432-6775 (FAX)
bin.ma@yale.edu

Colloquium: Laminar flames

Running Title: Soot formation in microgravity and normal gravity

Paper Length:

Total of 5754 words based on method 1
Main text: 3607
Figures: 261+200+582+150+134
Caption: 145
Equations: 53
References: 612

Affirmation: We will cover the cost of the color reproduction charges

Supplemental: Supplemental material has been made available.

Abstract

Upon the completion of the Structure and Liftoff in Combustion Experiment (SLICE) in March 2012, a comprehensive and unique set of microgravity coflow diffusion flame data was obtained. This data covers a range of conditions from weak flames near extinction to strong, highly sooting flames, and enabled the study of gravitational effects on phenomena such as liftoff, blowout and soot formation. The microgravity experiment was carried out in the Microgravity Science Glovebox (MSG) on board the International Space Station (ISS), while the normal gravity experiment was performed at Yale utilizing a copy of the flight hardware. Computational simulations of microgravity and normal gravity flames were also carried out to facilitate understanding of the experimental observations. This paper focuses on the different sooting behaviors of CH_4 coflow jet flames in microgravity and normal gravity. The unique set of data serves as an excellent test case for developing more accurate computational models. Experimentally, the flame shape and size, lift-off height, and soot temperature were determined from line-of-sight flame emission images taken with a color digital camera. Soot volume fraction was determined by performing an absolute light calibration using the incandescence from a flame-heated thermocouple. Computationally, the MC-Smooth vorticity-velocity formulation was employed to describe the chemically reacting flow, and the soot evolution was modeled by the sectional aerosol equations. The governing equations and boundary conditions were discretized on an axisymmetric computational domain by finite differences, and the resulting system of fully coupled, highly nonlinear equations was solved by a damped, modified Newton's method. The microgravity sooting flames were found to have lower soot temperatures and higher volume fraction

than their normal gravity counterparts. The soot distribution tends to shift from the centerline of the flame to the wings from normal gravity to microgravity.

Keywords: microgravity flame, soot temperature, soot volume fraction

1. Introduction

Microgravity is a unique environment in which to study combustion. The absence of buoyancy results in a simplified flow field that can serve as a "cleaner" test case to develop computational models. Highly diluted flames that extinguish in normal gravity (1 g) can be stabilized in microgravity (μ g), which enables the study of flames near extinction. Sooty flames with enhanced residence time can be also generated, which can be used to further study soot formation mechanisms. In general, the contrasting effects in normal and microgravity provide an excellent test case for developing an improved understanding of the factors that affect flame lift-off distance, extinction, and soot formation mechanisms. To better understand the factors that affect flame extinction and particulate formation, flames were investigated in the SLICE experiment on board the ISS. Although the SLICE experiment investigated flames with a wide dilution spectrum, from weak to highly sooting, the work described here emphasizes the sooting behaviors of coflow jet flames in microgravity and normal gravity.

The effect of gravity on soot formation has been studied over the past few decades. Experimentally, Greenberg *et al.* [1] conducted a reduced-gravity experiment in the NASA Glenn 2.2 s drop tower, and reported the first normal gravity and microgravity comparison of soot volume fraction for laminar acetylene and nitrogen-diluted acetylene jet diffusion flames. A factor of 2 to 4 increase in peak soot volume fraction was reported from 1 g to μ g. Walsh *et al.* [2] found that the laser induced incandescence (LII) signal of a methane coflow laminar diffusion flame increased by a factor of 15 during a parabolic flight. Jeon and Choi [3] studied the buoyancy effect on soot formation in a gas-jet diffusion flame in partial gravity conditions from 0.3 g to 1 g. The soot volume

fraction was measured by extinction and found to increase with reduced gravity level. Riemann *et al.* [4] performed LII in a drop tower, measuring both soot concentration and primary particle size. In microgravity, the maximum soot particle size is roughly double that of the 1-g case. Diez *et al.* [5] studied the properties of non-buoyant, laminar jet diffusion flames on board the Space Shuttle Columbia and showed the existence of a soot property-state relationship for such flames. Computationally, Kaplan *et al.* [6] simulated an ethylene-air diffusion flame and found that the peak soot volume fraction increased by a factor of 10 from 1 g to μ g. Their simulation did not reach steady-state conditions within ~ 3 s of microgravity. This result indicates that flames may not stabilize in short-duration drop tower experiments. Kong and Liu [7] recently simulated laminar coflow methane/air diffusion flames and studied the effects of the air coflow velocity. The peak soot volume fraction in microgravity was found to be about twice that in normal gravity [8]. Liu *et al.* [9] computed the influence of heat transfer and radiation on the structure and soot formation characteristics of a coflow laminar ethylene/air diffusion flame and showed that radiative heat loss plays a major role in the flame structure in microgravity. Charest *et al.* [10] recently simulated the influence of gravity on a laminar coflow methane/air diffusion flame, demonstrating that the μ-g flame has lower gas temperatures, thicker soot regions and higher soot volume fractions than the 1-g flame.

Although significant efforts have been made to experimentally study gravitational effects on soot formation processes, there are some uncertainties and complications associated with experiments. For example, flames in short-duration drop tower experiments are often not fully stabilized; on the other hand, the gravitational-jitter in parabolic flight can dramatically disturb low-momentum flames, affecting the accuracy

of the measurements. Furthermore, the experimental results are quite limited due to the sheer cost of the microgravity experiments. Many computational studies have been conducted, but they were performed for conditions different from the available experimental data. Therefore, no direct comparison between experiment and computation was available for microgravity flames, making it hard to directly assess the effectiveness of the computational models. The SLICE project, on the other hand, is a joint experimental and computational study. The microgravity tests were conducted by crewmember Dr. Donald R. Pettit in 2012 in the Microgravity Science Glovebox (MSG) on board the ISS, which provides a stable microgravity environment for conducting long-duration experiments. The normal gravity SLICE experiment was performed at Yale, using a replica of the SLICE flight hardware (namely, the engineering and training hardware). Detailed near-field velocity measurements performed on the engineering unit guided the boundary conditions used in the computations. In the following sections, two-dimensional comparisons of 1-g and μ-g soot temperature and volume fraction are presented from both experiment and computation.

2. SLICE experimental setup

The basic SLICE experimental setup was originally used in the Enclosed Laminar Flames (ELF) investigation [11] to study the effect of buoyancy on the stability of coflow gas-jet diffusion flames during the STS-87 Space Shuttle mission. A schematic of the SLICE burner inside the hardware is shown in Fig. 1. The duct has a 76 mm × 76 mm square cross-section with rounded corners and is 174 mm tall. The central fuel jet tube has a threaded base that allows five nozzles with 0.41, 0.77, 1.59, 2.14 and 3.23 mm inner diameter to be interchanged. The fuels used in SLICE include 100% CH_4, 70% CH_4, 40%

CH_4, 100% C_2H_4 and 20% C_2H_4 (by volume) diluted with N_2. The current study focuses on 100% CH_4/air laminar diffusion jet flames using 1.59 mm and 3.23 mm fuel nozzles. The fuel flow rate was controlled by a mass flow controller and could be adjusted manually in the range of 0-500 sccm N_2 equivalent flow.

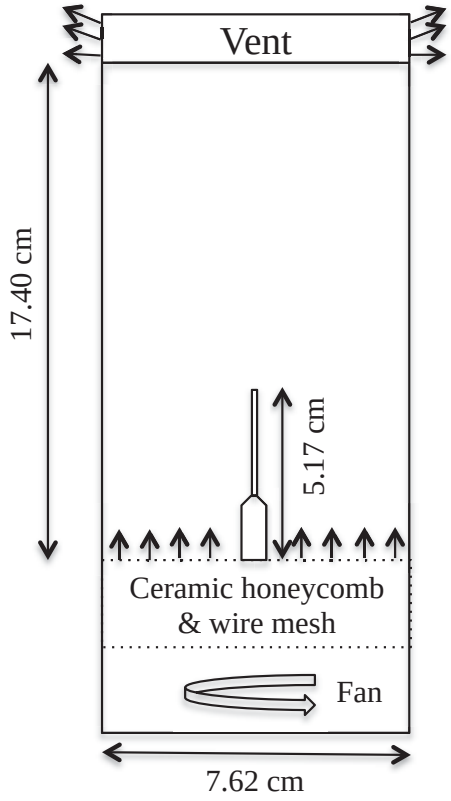

Fig. 1. SLICE burner configuration.

As shown in Fig. 1, coflow air is supplied by a DC fan located at the upstream end of the duct. The coflow air passes through a honeycomb and a wire mesh to straighten the flow and flatten the velocity profile before entering the duct. The coflow air velocity is varied by changing the fan voltage. An omni-directional hot-sphere anemometer between the honeycomb and mesh provides a reference measurement for the air velocity. The flow field of the coflowing air was measured in the engineering unit at

different fan voltage levels using a thin (~ 3.8 μm) hot-wire anemometer at the height of 1 mm above the 1.59 mm fuel nozzle by scanning through the width of the duct. The scanning step is 2 mm in the far field where the coflow velocity gradient is small and 0.5 mm close to the burner where the gradient is large. The measured velocity profiles are shown in the supplemental material. Due to hardware imperfections, the coflow near the fuel nozzle is not perfectly symmetric. The velocities of the two sides were averaged around the burner axis and used to establish the boundary condition for the 2-D simulations. Although the flight and engineering units are very similar and steps were taken to match conditions as closely as possible between the two, differences in the details of the velocity profiles between the two pieces of hardware are possible. In comparing results between normal gravity and microgravity, as well as between measurements and computations, these uncertainties should be kept in mind. An analog color video camera was used to monitor the flame behavior. Several test conditions, including fuel flow rate, fan setting, anemometer reading and a timer, were superimposed on the video. In post-processing, an optical character recognition algorithm was used to analyze the video to automatically obtain the test conditions and time from the recorded video. Still images were taken by a digital single lens reflex (DSLR) camera (Nikon D300s)[1] with a 2 mm BG-7 filter attached in front of the lens. The filter was used to balance the red, green, and blue (RGB) channels of the acquired color images. The normal test procedure involved manually setting the desired flow conditions and taking images in bracket mode to ensure unsaturated images were obtained. The camera exposure time and *f*-number were typically set based on prior ground and microgravity

[1] The product reference was provided for clarity and does not represent an endorsement on the part of NASA or the federal government.

test. For each still image captured by the Nikon camera, the corresponding test conditions were determined by matching the video time to the image time available in the EXIF (EXchangeable Image Format) data, which can be read out by the image processing software OMA [12].

3. Soot diagnostics

A color-ratio pyrometry approach based on a color DSLR camera, which was developed and discussed in [13, 14], was used in this study. The DSLR camera was fully characterized and used as a color-ratio pyrometer. The coupled spectral response of the camera and BG-7 filter was measured and is similar to the one reported in [14], although the SLICE's BG-7 filter has lower red light transmission. Lookup tables correlating temperature and color-ratio were generated by integrating soot spectral emissivity over the camera spectral responses as shown by Eq. (1):

$$\frac{S_{F_1}}{S_{F_2}} = \frac{\int \eta_{F_1}(\lambda)\varepsilon(\lambda)I_{BB}(\lambda,T)d\lambda}{\int \eta_{F_2}(\lambda)\varepsilon(\lambda)I_{BB}(\lambda,T)d\lambda}, \quad \text{Eq. (1)}$$

where S_{F_i} is the calculated signal for the i^{th} channel, η_{F_i} is the spectral response of the i^{th} channel, $\varepsilon(\lambda)$ is the soot spectral emissivity as a function of wavelength λ, and $I_{BB}(\lambda,T)$ is the spectral radiance of a black body at wavelength λ and temperature T as calculated by Planck's radiation law. The soot emissivity was normally assumed to vary with wavelength as shown in Eq. (2) with α being the so-called dispersion exponent.

$$\varepsilon(\lambda) \propto \lambda^{-\alpha}, \quad \text{Eq. (2)}$$

The value of α is fundamentally important to color-ratio pyrometry as it represents the underlying assumptions of the soot spectral emissivity model and affects the calculated lookup tables. The value is considered to be dependent on the soot aging stages and has been measured in several studies with a range of value from 0.5 to 2.2 reported for various flame conditions. Mature soot with a higher C/H atom ratio was found to have smaller α values and young soot has greater α values [15-18]. A recent study [19] performed 2-D measurements of α across the sooty region in a normal gravity N_2-diluted 80% C_2H_4 coflow laminar diffusion flame. For that case, the measured value of α was found to be as small as 0.9 on the flame wings and as large as 1.4 on the flame centerline. This trend is in agreement with the literature since soot on the flame wings is expected to be more mature with higher C/H ratios and therefore has a smaller value of α. In Ref. [19], the spatially resolved 2-D α map was then used in conjunction with color-ratio pyrometry to determine the soot temperature. Although it would be desirable to use a 2-D α map rather than a constant nominal value, it was not possible to measure α in this study. Therefore, consistent with previous studies [13], $\alpha = 1.38$ is assumed for all the flames. It should be kept in mind that the derived soot temperature based on a single nominal α value may deviate from the true temperature especially in regions with different α values such as the flame wings. The effect of α variation on the soot temperature and volume fraction will be discussed in Section 5.

The image processing was performed using the open source software OMA [12]. Each flame image was separated into three RGB images and then converted to radial profiles using an Abel inversion. The soot temperature can then be determined by

applying the soot lookup table to the ratio images of the radial profiles. In order to reduce unphysical temperatures caused by low signals and noisy ratios, a spatial filter was created based on the inverted intensity image and used to cut off areas with signal values less than 10% of the maxima. Details of the image processing and temperature determination can be found in the original paper describing the technique [13]. Once the soot temperature is determined, the soot volume fraction can be obtained through an absolute light intensity calibration. Absolute light intensity calibration is used to quantify the geometric factors and optical transmission associated with the specific setup. The traditional calibration sources such as a blackbody source or a tungsten lamp cannot fit in the SLICE duct due to their large volume; as an alternative solution, a novel light calibration approach using an S-type thermocouple, which can be easily placed in small volumes given its small size, was developed [20]. The spectral emissivity of both the platinum and platinum/rhodium wires used to manufacture the S-type thermocouple was measured in the visible range. The incandescence of the flame-heated thermocouple can then be calculated based on Planck's radiation law given the measured emissivity and thermocouple temperature reading, and was used as the calibration source to quantify the soot volume fraction. The details of the calibration procedure are described in Refs. [13, 20].

4. Computational approach

The MC-Smooth vorticity-velocity formulation [21] of the governing equations is employed to simulate each flame, with the chemically reactive mixture treated as Newtonian, the diffusion of each species approximated as Fickian, the divergence of the net radiative flux evaluated by an optically thin radiation model [22-24], and the

evolution of soot particles represented by a sectional model [25-28] with 20 sections. The gas-phase chemistry contains 42 species and 250 reactions, which is based on the GRI 3.0 mechanism [29] with all nitrogen-containing species (except N_2) removed and a series of reactions related to the formation and oxidation of benzene and associated species (see Table 1 of [25]) added. Since each flame is axisymmetric, a 2-D computational domain with r_{max} = 4.29 cm and z_{max} = 12.20 cm is employed, with all boundary conditions selected to match experimental conditions. The square duct is approximated as a coaxial tube with an identical cross-sectional area. The domain is spanned by a nonuniform 129 × 202 tensor product grid. The governing equations and boundary conditions are discretized on this grid via nine-point finite difference stencils. The resulting set of fully coupled, highly nonlinear equations is then solved simultaneously at all grid points using a damped modified Newton's method [30, 31] with a nested Bi-CGSTAB linear algebra solver [32], and each flame is solved to a Newton tolerance of 10^{-4}. Further information on the computational approach can be found in a companion paper [33].

5. Results and discussion

A 100% CH_4 flame using 3.23 mm ID nozzle with average fuel velocity of 46 cm/s and nominal air coflow of 18 cm/s was measured at 1 g and μ g. Digital color images of both flames are shown in Fig. 2. The fact that the color images appear green is due to a BG-7 filter is attached in front of the lens to balance the RGB signal, e.g., preventing saturation in the red channel. Soot temperatures were determined from these color images using the color-ratio pyrometry technique. Soot volume fractions were then

obtained given the measured temperature and the absolute light calibration using an S-type thermocouple as mentioned in Section 3.

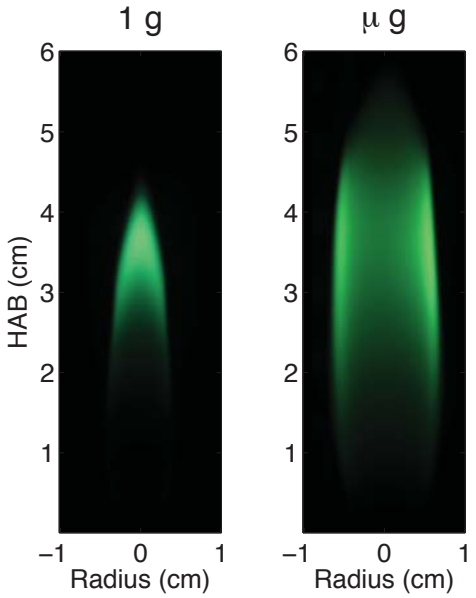

Fig. 2. Digital color images of 1-g (left) and μ-g (right) flames taken through the BG-7 filter under the specified flow conditions. The vertical coordinate is height above the burner surface.

The measured soot temperature and volume fraction are shown in the top row of Fig. 3. In μ g, a taller and wider flame was produced and the peak soot volume fraction increased by a factor of ~ 8. The enhanced soot production resulted in increased thermal radiation losses and hence reduced flame temperatures. The peak soot temperature in μ g is shown to be ~ 200 K lower than its 1 g counterpart. From 1 g to μ g, the peak of soot volume fraction was also redistributed from the flame centerline to the wings. The soot growth mode is believed to change from an inception-dominated mode to a surface-growth-dominated mode [28]. Computational simulations were also carried out for the flame. The simulated soot temperature and volume fraction of the same flame are shown

in the bottom row of Fig. 3. From 1 g to μ g, the flame shape and the shift of soot from the centerline at 1 g to the wings at μ g is very well predicted. While making comparisons between experiment and computation, it should be noted that the measured soot profile shown here is only plotted in regions with good signal-to-noise ratio. It does not necessarily suggest there is no soot along the centerline below 5 cm height above the burner (HAB) in the μ g flame. On the computed soot volume fraction map, residence time contours are also superimposed. The residence time in milliseconds is determined based on the simulated axial velocities as shown in Fig. 4 where the radial velocities are neglected given their much smaller magnitude. Due to the buoyancy effect, the hot flow under 1 g is accelerated and the maximum velocity is up to ~ 200 cm/s at the far downstream location, while the μ g maximum velocity is only ~ 90 cm/s at the upstream location around the tip of the burner given the parabolic fuel velocity profile. Compared to the 1-g flame, the μ-g counterpart is more diffusion-controlled and has thicker diffusion layers with more soot production in the wings. The reduction in axial velocity results in longer residence times, and allows more time for soot particles to grow and results in an enhanced soot volume fraction. The simulation qualitatively captures the trend. However, the quantitative agreement between experiment and computation is not good. In 1 g, the predicted soot volume fraction has the same order of magnitude as the measured value. However, the computation does not capture the dramatic increase in soot volume fraction from 1 g to μ g. It should be noted that the current computational model uses an optically thin radiation assumption that does not account for radiation reabsorption. This may affect prediction of soot temperature, and more importantly, soot volume fraction, given its great sensitivity to temperature. A previous study [27] has

shown that the simulated soot volume fraction is greater when reabsorption is considered. The effect of reabsorption is expected to be more important in microgravity given the longer residence time and higher soot volume fraction.

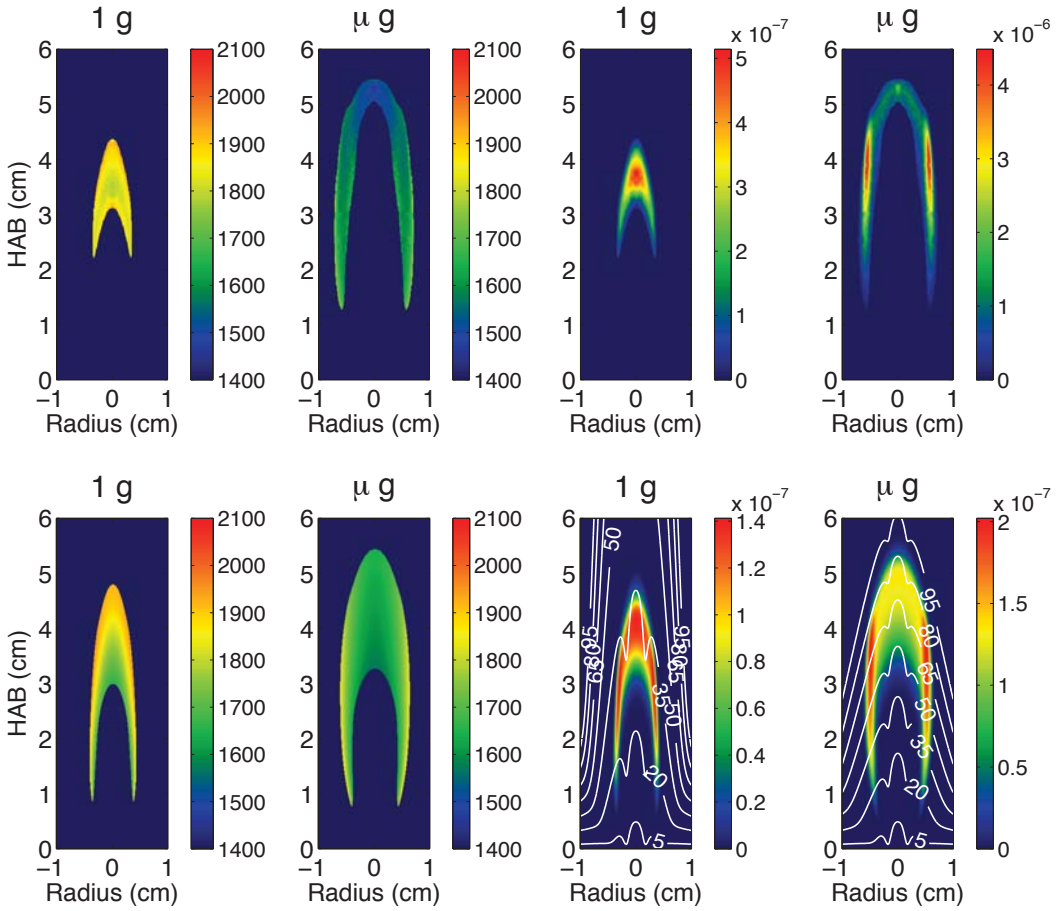

Fig. 3. (Top) Measured 1-g and μ-g soot temperature comparison (left) and soot volume fraction comparison (right) for a 100% CH_4 flame with 3.23 mm ID nozzle. Average fuel speed is 46 cm/s and coflow speed is nominally 18 cm/s. (Bottom) Computed quantities corresponding to the measurements above. Residence time contours (milliseconds) are superimposed on the calculated soot volume fraction maps.

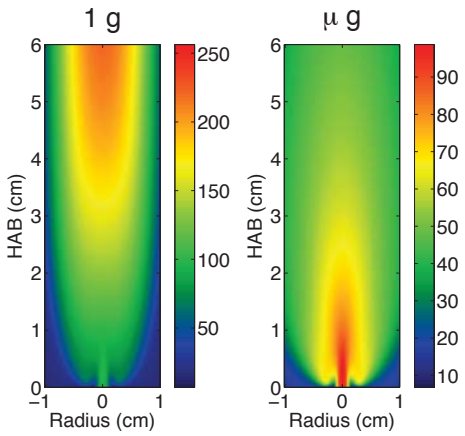

Fig. 4. 1-g and μ-g computed axial velocity comparison [cm/s] in a 100% CH_4 flame with 3.23 mm ID nozzle. Average fuel speed is 46 cm/s and coflow speed is nominally 18 cm/s.

While making quantitative comparisons between experiment and computation, it is important to reflect on the measurement uncertainties. As mentioned above, the soot dispersion exponent α is assumed to be the same for normal gravity and microgravity flames. This may not be true since the microgravity soot with longer residence time is expected to be more "mature" and thus to have a smaller value of α. The effect of α on measured temperature and soot volume fraction in the μ-g flame is plotted in Fig. 5, where the temperature and soot volume fraction at the peak soot volume location are plotted as a function of α. While the true soot dispersion exponent remains unknown in microgravity, a range from 0.9 to 1.38 is estimated based on literature values [15-18] and our previous investigation [19]. As the value of α increases from 0.9 to 1.38, the derived temperature is shown to decrease from ~ 1622 K to ~ 1575 K and the soot volume fraction is shown to increase from ~ 2.6 ppm to ~ 4.5 ppm. The derived soot volume fraction is affected more strongly, because temperature appears in the exponential term in

Planck's radiation equation. By considering the estimated range of the soot dispersion exponent α from 0.9 to 1.38, the measured microgravity soot temperature is possibly underestimated by up to ~ 50 K, and the measured microgravity soot volume fraction is possibly overestimated by up to a factor of nearly 2. From 1 g to μ g under the current flow conditions, the peak soot volume fraction is shown to increase by a factor of approximately 4 to 8 bounded by the uncertainty in soot dispersion exponent in microgravity.

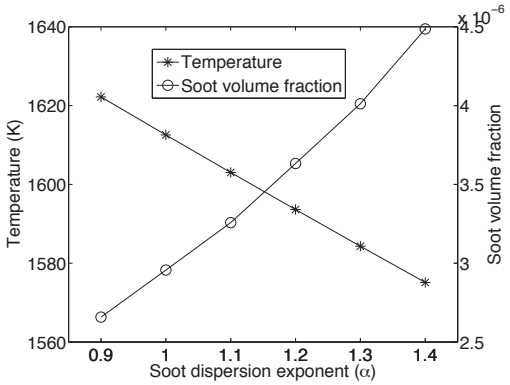

Fig. 5. The effect of soot dispersion exponent α on measured temperature and soot volume fraction at the position with peak soot volume fraction.

More normal gravity and microgravity CH_4 flames have been measured. In order to make the data more widely available and facilitate computations using other codes, the data files of soot temperature and volume fraction and their corresponding boundary conditions are made available in the supplemental materials. Example Matlab code to read and plot data is also attached.

6. Conclusions

A unique set of CH_4/air coflow laminar diffusion flames were measured and

computed in normal gravity and microgravity as part of the SLICE project to investigate the gravitational effects on sooting behaviors in these flames. The ISS provided a stable microgravity environment for conducting long-duration, high-quality microgravity combustion measurements. From the experiments, the microgravity flames were found to be sootier than normal gravity flames by a factor of approximately 4 to 8 in terms of the peak soot volume fraction (based on the uncertainty of the soot dispersion exponent and temperature measurements). The distribution of peak soot was also found to shift from the centerline of the flame at 1 g to the wings at μ g. The flame temperature in μ g is shown to be lower than its 1-g counterpart due to higher soot loading and radiative loss. Computations of both 1-g and μ-g flames yield good agreement in flame shape with experimental results. The computational model also successfully captured the soot migration from the centerline at 1 g to the wings at μ g. However, the soot volume fraction is underestimated, especially in microgravity. Accurate prediction of the soot volume fraction remains a challenge. Advanced reabsorption submodels will be introduced in the future to better predict soot temperature and volume fraction. More measured and computed temperature and soot volume fraction data files at different flow conditions and their corresponding boundary conditions are made available in the supplemental material.

7. Acknowledgements

This research was supported by NASA under contract NNX11AP43A. The authors would like to thank astronaut Don Pettit for conducting SLICE's microgravity tests, SLICE Project Manager Bob Hawersaat, and operations team members Chuck Bunnell, Tibor Lorik, Jay Owens and Carol Reynolds.

8. References

1. P. S. Greenberg, J. C. Ku, Combust. Flame 108 (1–2) (1997) 227-230.
2. K. T. Walsh, J. Fielding, M. D. Smooke, M. B. Long, Proc. Combust. Inst. 28 (2000) 1973-1979.
3. B.-H. Jeon, J. Choi, J Mech Sci Technol 24 (7) (2010) 1537-1543.
4. J. Reimann, S.-A. Kuhlmann, S. Will, Microgravity Sci. Technol. 22 (4) (2010) 499-505.
5. F. J. Diez, C. Aalburg, P. B. Sunderland, D. L. Urban, Z. G. Yuan, G. M. Faeth, Combust. Flame 156 (8) (2009) 1514-1524.
6. C. R. Kaplan, E. S. Oran, K. Kailasanath, H. D. Ross, Proc. Combust. Inst. 26 (1) (1996) 1301-1309.
7. W. Kong, F. Liu, Combustion Theory and Modelling 13 (6) (2009) 993 - 1023.
8. W. J. Kong, F. S. Liu, Microgravity Sci. Technol. 22 (2) (2010) 205-214.
9. F. Liu, G. J. Smallwood, W. Kong, Journal of Quantitative Spectroscopy and Radiative Transfer 112 (7) (2011) 1241-1249.
10. M. R. J. Charest, C. P. T. Groth, Ö. L. Gülder, Combust. Flame 158 (5) (2011) 860-875.
11. J. E. Brooker, K. Jia, D. P. Stocker, L.-D. Chen, Proceedings of the Fifth International Microgravity Combustion Workshop (1999) 97-100.
12. P. A. M. Kalt, M. B. Long, http://www.oma-x.org (2013).
13. P. B. Kuhn, B. Ma, B. C. Connelly, M. D. Smooke, M. B. Long, Proc. Combust. Inst. 33 (1) (2011) 743-750.
14. B. Ma, G. Wang, G. Magnotti, R. S. Barlow, M. B. Long, Combust. Flame (0) (In press). http://dx.doi.org/10.1016/j.combustflame.2013.10.014
15. C. R. Shaddix, Á. B. Palotás, C. M. Megaridis, M. Y. Choi, N. Y. C. Yang, Int. J. Heat Mass Transfer 48 (17) (2005) 3604-3614.
16. H. Zhao, N. Ladommatos, Prog. Energy Combust. Sci. 24 (3) (1998) 221-255.
17. A. D'Alessio, F. Beretta, C. Venitozzi, Combust. Sci. Technol. 5 (1) (1972) 263-272.
18. R. C. Millikan, J. Opt. Soc. Am. 51 (6) (1961) 698-699.
19. B. Ma, M. B. Long, Appl. Phys. B (submitted).
20. B. Ma, M. B. Long, Proc. Combust. Inst. 34 (2) (2013) 3531-3539.
21. S. Cao, B. A. V. Bennett, M. D. Smooke, (in preparation).
22. D. K. Edwards, Adv. Heat Transfer 12 (1976) 115–193.
23. R. J. Hall, Journal of Quantitative Spectroscopy and Radiative Transfer 51 (4) (1994) 635-644.
24. R. J. Hall, Journal of Quantitative Spectroscopy and Radiative Transfer 49 (5) (1993) 517-523.
25. R. J. Hall, M. D. Smooke, M. B. Colket, in: Physical and Chemical Aspects of Combustion: A Tribute to Irvin Glassman (R.F. Sawyer and F.L. Dryer, Eds.), Combustion Science and Technology Book Series, Gordon and Breach: Amsterdam, 1997.
26. M. D. Smooke, C. S. McEnally, L. D. Pfefferle, R. J. Hall, M. B. Colket, Combust. Flame 117 (1-2) (1999) 117-139.

27. M. D. Smooke, R. J. Hall, M. B. Colket, J. Fielding, M. B. Long, C. S. McEnally, L. D. Pfefferle, Combustion Theory and Modelling 8 (3) (2004) 593-606.
28. M. D. Smooke, M. B. Long, B. C. Connelly, M. B. Colket, R. J. Hall, Combust. Flame 143 (4) (2005) 613-628.
29. G. P. Smith, D. M. Golden, M. Frenklach, N. W. Moriarty, B. Eiteneer, M. Golderberg, C. T. Bowman, R. K. Hanson, S. Song, W. C. Gardiner, V. V. Lissianski, Z. Qin, GRI-Mech 3.0; available at http://www.me.berkeley.edu/gri_mech (1999).
30. P. Deuflhard, Numerische Mathematik 22 (4) (1974) 289-315.
31. M. D. Smooke, Journal of Optimization Theory and Applications 39 (4) (1983) 489-511.
32. H. A. Van der Vorst, SIAM Journal on Scientific and Statistical Computing 13 (2) (1992) 631-644.
33. S. Cao, B. Ma, B. A. V. Bennett, D. Giassi, D. P. Stocker, F. Takahashi, M. B. Long, M. D. Smooke, Proc. Combust. Inst. (submitted).

Fig. 1. SLICE burner configuration.

Fig. 2. Digital color images of 1-g (left) and m-g (right) flames taken through the BG-7 filter under the specified flow conditions. The vertical coordinate is height above the burner surface.

Fig. 3. (Top) Measured 1-g and μ-g soot temperature comparison (left) and soot volume fraction comparison (right) for a 100% CH_4 flame with 3.23 mm ID nozzle. Average fuel speed is 46 cm/s and coflow speed is nominally 18 cm/s. (Bottom) Computed quantities corresponding to the measurements above. Residence time contours (milliseconds) are superimposed on the calculated soot volume fraction maps.

Fig. 4. 1-g and μ-g computed axial velocity comparison [cm/s] in a 100% CH_4 flame with 3.23 mm ID nozzle. Average fuel speed is 46 cm/s and coflow speed is nominally 18 cm/s.

Fig. 5. The effect of soot dispersion exponent α on measured temperature and soot volume fraction at the position with peak soot volume fraction.